2.18 Beam-Based Longitudinal and Transverse Impedance/Instability Measurements

G. Rumolo, E. Shaposhnikova
CERN, 1211 Geneva 23, Switzerland
Mail to: Giovanni.Rumolo@cern.ch

2.18.1 Introduction

The wake function of an accelerator device is defined as the integral along the full electromagnetic length of the device of the electromagnetic force generated by a point charge going through the device at the speed of light and acting on a witness point charge placed at a distance z from the source. For the longitudinal plane, both source and witness are assumed to be traveling on axis – usually defined by the symmetry axis of the device, or by the closed orbit trajectory when the device is placed in an accelerator. For the transverse plane (horizontal and vertical), one has to consider offsetting either the source particle (dipolar wake) or the witness particle (quadrupolar wake) by an arbitrarily small amount, and redefine the wake as the electromagnetic force normalised to the given offset. The beam coupling impedance is the Fourier transform of the wake function (additionally multiplied by the imaginary unit i in the case of the transverse impedance) and therefore describes the same type of interaction in the frequency domain. Note that, due to the normalisation to the offset in the definitions, transverse wakes/impedances have an additional m^{-1} in the dimensions with respect to their longitudinal counterparts. Due to the validity of superposition and if one assumes that adjacent devices can be considered electromagnetically decoupled, the beam coupling impedance of a sequence of devices turns out to be a simple weighted sum of the beam coupling impedances of the single devices. The weights are given by the optical beta functions at the locations of the devices for the horizontal and vertical impedances, while they are just unitary for the longitudinal impedances. A full accelerator ring can be described through a global beam coupling impedance, which represents the beta function weighted sum of the beam coupling impedances of its individual components in the transverse plane and their simple sum in the longitudinal plane (see Section 2.9). While wake functions are widely used in macroparticle simulations to express the driving terms representing the electromagnetic interaction of the beam in the equations of motion of the single macroparticles, beam coupling impedances are commonly used to describe electromagnetically single devices and make comparative studies. Furthermore, since analytical models usually solve the beam equations in frequency domain, global or individual beam coupling impedances can also be fed in handy formulae to estimate quantities like power loss, synchronous phase shift, betatron and synchrotron tune shifts and instability/damping rates in controlled operating conditions. Beam coupling impedances of single devices can be measured either in a laboratory prior to their installation in a machine (see Section 2.8) or with beam directly in the accelerator in which they are installed, using specific local techniques, some of which will be shortly addressed in one of the next subsections. The global beam coupling impedance of an accelerator can be estimated using techniques based on direct global beam observables, like the quantities listed above, for which simplified analytical expressions exist. Different techniques have to be used to estimate separately the real and the imaginary parts of the impedance, while different frequency ranges can be probed according to the beam parameters used in the measurement, as will be explained in this chapter at a later stage.

In the following subsections, we will solely focus on the review of a subset of the most common existing techniques to measure the beam coupling impedance of a full accelerator ring based on global beam measurements. However, it is worth mentioning briefly at this stage that there exist also techniques to estimate the impedance of single components with beam. Here are some examples:

- Differential global measurements can be used for elements that can be moved in and out, like collimators, scrapers, experimental insertions, movable diagnostics, or in-vacuum undulators. The contribution to the impedance given by these elements in their 'in' position can be evaluated by difference measuring the global impedance of the ring when they are retracted and when they are inserted.
- Global impedance measurements can also be made in the same beam conditions before and after the installation of a certain element into an accelerator ring. This provides a direct estimation of the impedance of the element installed. For both this case and the case above, this type of measurement is possible only if the relative contribution of the device under test to the global impedance of the ring is high enough to be detectable within the accuracy of the measurement.
- Another technique that has been attempted in many accelerators is the transverse impedance localisation through the measurement of the shift of the phase advance between successive beam position monitors with intensity. This method is expected to provide information about the detailed breakdown of the total impedance of a machine over its elements and identify at least the most significant contributors.
- The longitudinal impedance of a certain element can be directly estimated if the beam induced heating of this element can be measured. This is usually the case for devices like ferrite kickers, whose temperature is monitored to prevent them from overheating and reaching the Curie temperature, or cold vacuum chambers or pieces of equipment, e.g. in superconducting magnets (like the LHC beam screen) or superconducting RF cavities.

It should be noted that in many cases the impedance model of a device or a machine is also built independently via electromagnetic simulations and/or bench measurements (ideally, already in the design phase of the accelerator to predict its perfomance), and then simply validated through beam based measurements. For completeness, in the next sections we will always illustrate selected applications of the various methods to running accelerators.

2.18.2 **Transverse Impedance Measurements with Beam**

2.18.2.1 ***Tune Shifts with Intensity and Instability Growth Rates with Chromaticity***

The kinetic theory based on the solution of the Vlasov equation can be applied to a single bunch under the effect of a dipolar transverse wake/impedance and the evolution of the bunch distribution function in phase space can be resolved resorting to mode decomposition. In particular, it can be demonstrated that, for sufficiently low intensity values, any coherent transverse oscillation of a single Gaussian bunch circulating in a given machine can be decomposed into an infinity of modes, whose frequencies are given by the following formula [1]:

$$\Omega^{(l)} - \omega_\beta - l\omega_s \approx -\frac{i}{4\pi}\frac{\Gamma(l+\frac{1}{2})}{2^l l!}\frac{Ne^2\bar{\beta}_{x,y}}{m_0\gamma C\sigma_z}\frac{\sum_{p=-\infty}^{\infty} Z_1^{\perp}(\omega')h_l(\omega'-\omega_\xi)}{\sum_{p=-\infty}^{\infty} h_l(\omega'-\omega_\xi)} \tag{1}$$

where l is the mode number, C is the circumference of the accelerator, ω_β is the betatron frequency (i.e. the machine tune $Q_{x,y}$ multiplied by the revolution frequency $\omega_0 = 2\pi c/C$), ω_s is the synchrotron frequency (i.e. the synchrotron tune Q_s multiplied by the revolution frequency $\omega_0 = 2\pi c/C$), N is the number of particles in the bunch, $\bar{\beta}_{x,y}$ is the average beta function of the accelerator, γ is the relativistic factor, σ_z is the rms bunch length, $Z_1^{\perp}(\omega)$ is the global transverse impedance of the machine, $h_l(\omega)$ are the spectra of the different modes of the Gaussian bunch, given by the following equation:

$$h_l(\omega) = \left(\frac{\omega\sigma_z}{c}\right)^{2l}\exp\left(-\frac{\omega^2\sigma_z^2}{c^2}\right) \tag{2}$$

ω' is defined by

$$\omega' = p\omega_0 + \omega_{\beta x,y} + l\omega_s \tag{3}$$

ω_ξ is the chromatic frequency defined by:

$$\omega_\xi = \frac{\xi_{x,y}\omega_{\beta x,y}}{\eta} \tag{4}$$

η is the slippage factor of the accelerator, which depends on the momentum compaction factor α and the relativistic factor γ according to

$$\eta = \alpha - \frac{1}{\gamma^2} \tag{5}$$

With this convention, η is positive if the accelerator ring is operated below transition ($\gamma < 1/\sqrt{\alpha}$) and it is negative above transition. The modes given by Eq. (1) are called 'azimuthal modes'. In reality, for each azimuthal mode there exists also an infinity of 'radial modes', but this can be neglected in the regime we are considering. To be noted that the last fraction present at the RHS of Eq. (1), featuring at the numerator the weighted summation of the sampled transverse impedance multiplied by the bunch modal spectrum (shifted by the chromatic frequency), is usually defined as effective impedance Z_{eff} and does not depend on frequency.

From Eq. (1) we can derive two possible classes of observables:

1) If the chromaticity is zero, the l=0 mode represents a pure centroid (rigid bunch) oscillation. Its frequency is purely real and depends solely on the imaginary part of the

impedance. The LHS of Eq. (1), divided by the revolution frequency, reduces to the coherent betatron tune shift of the bunch. It can be measured in practice by exciting the bunch (by means of a kick or continuous excitation) and determining the deviation of its tune, as obtained by Foutier analysing the turn-by-turn data acquired with a position pick up, from the nominal tune of the machine (zero intensity tune). This measurement can be repeated for different intensities and the measured slope $\mathrm{Re}(\Delta\Omega)/(N\omega_0)$ would provide direct information about the effective transverse impedance. It is important to point out here that the slope of the coherent tune shift with intensity is always negative because the summation at the numerator of the LHC of Eq. (1) reduces to *i* times a positive quantity (this can be demonstrated from the properties of the impedances). Physically, this means that the effect of an impedance on a bunch is always globally defocusing. Modes with l≠0 represent components of the bunch oscillation accounting for the relative dephasing between head and tail. These modes exist also in absence of chromaticity, as they are introduced by the synchro-betatron coupling due to the beam coupling impedance itself – and the formula above would provide their shift with intensity similarly to mode l=0. However, since they are usually very weak and difficult to detect, the shift with intensity of high order headtail modes is not a handy observable to make impedance estimations. In practice, these modes tend to become visible only for higher intensities, when Eq. (1) breaks down and adjacent modes tend to couple, giving rise to strong headtail instabilities. This will be covered to some extent in the next subsection. It is important to highlight at this stage that, although Eq. (1) was obtained by assuming in the model only the presence of a dipolar type of impedance, in reality the transverse impedance that can be inferred through the measurement of the coherent tune shift with intensity is what accelerator physisicts usually refer to as 'generalised impedance', i.e. the sum of the dipolar and quadrupolar components of the transverse impedance [2]. This has to be kept in mind when applying this method, as in most accelerators the quadrupolar component of the impedance is of the same order of magnitude as the dipolar component and its contribution to the tune shift is not negligible. This may result in either a significantly larger value of impedance with respect to what could be expected from a model based on dipolar impedances alone or in an almost zero impedance measured, as the quadrupolar component can have opposite sign with respect to the dipolar component and the two contributions to the coherent tune shift would therefore tend to cancel out.

2) If chromaticity is nonzero, the pattern of the l=0 mode is associated with a headtail dephasing and the oscillation frequency of this mode is complex. One can see that the imaginary part of this complex number, which only depends on the real part of the transverse impedance, is positive (growth rate, which is the inverse of the rise time) if chromaticity is negative above transition energy. In a similar fashion, this mode will be also unstable for positive chromaticy if the accelerator ring is operating below transition. The rise time of this instability can be measured for different chromaticity values providing not only an estimation of the resistive part of the impedance but also providing information on its frequency spectrum, roughly scanned via the change of the chromatic frequency. Usually, this mode is quite strong and its rise time is a clearly measurable quantity. Modes with l≠0 are headtail oscillations that tend to become unstable in a complementary fashion with respect to the l=0 mode (i.e. with positive chromaticty above transition and with negative chromaticity below transition). This is certainly true with impedances of resistive wall type, while the situation is

more complicated with broad-band types of impedances and depends on the bunch length and resonance frequency of the broad band resonator. Measurements of the growth rates of these high order headtail modes, usually possible in presence of a strong resistive wall impedance, are quite difficult in other cases, because they have long rise times for low intensities and can be easily stabilised by other mechanisms (e.g. Landau damping).

In the case of the growth rates of the headtail modes (of whatever order l), the mechanism that drives the instability is only linked to the dipolar impedance. As a consequence, the measurement can only reveal the real part of the dipolar component of the impedance, while no information on the quadrupolar component can be inferred using this method.

It is worth noting also that using short bunches (as low σ_z as possible) for the evaluation of Eq. (1) has the twofold benefit to i) produce potentially larger tune shifts with intensity and make the tune shift more easily detactable and freer from resolution errors; and ii) result in wider bunch spectra $h_l(\omega)$, sampling the impedance over a larger frequency span. An important implication of this simple fact is that measurements with different bunch lengths can be conducted to potentially assess the high frequency content of the impedance spectrum. If increasing the bunch length results in a tune shift with intensity scaling like the inverse of the bunch length, one could deduce that the transverse impedance spectrum does not extend significantly beyond the bandwidth of the longest bunch used in the measurements; if, conversely, the relation is more complicated, information on the integrated impedance spectrum in the ranges of frequency progressively covered by the different bunch spectra can be found.

Measurements of coherent tune shift with intensity for about constant bunch length carried out at the CERN Super Proton Synchrotron (SPS) in 2012 are displayed in Fig. 1 [3].

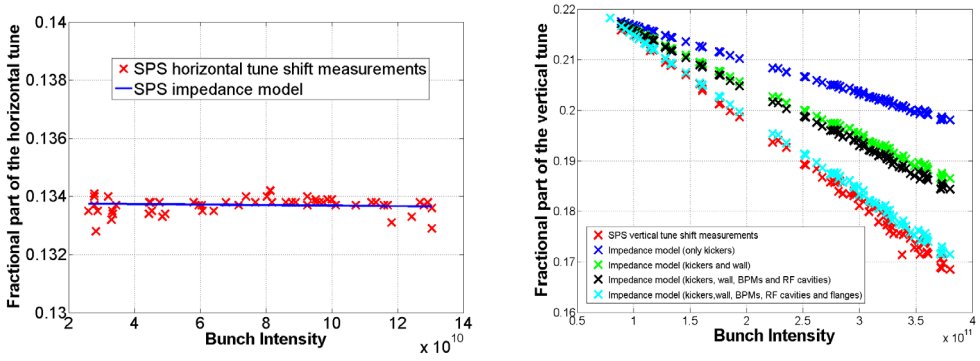

Figure 1: Fractional part of the horizontal (left) and vertical (right) tune as a function of the bunch intensity in the CERN SPS. The red crosses correspond to the measured points.

In both plots shown in Fig. 1, we can see the measured tunes at the different intensities (red crosses) as well as the calculations using the existing SPS impedance model, built from summing up the contributions of the individual elements (at least those deemed to be most significant in the global impedance assessment). In the case of the vertical plane, in addition, the breakdown of the different contributions to the global impedance model of the machine has been explicitly included. Looking at the different lines, one can easily deduce that the magnetic kickers are responsible for about 40% of the total vertical impedance for the SPS (blue crosses), the vacuum chamber wall for 20% (blue to green crosses), other components

– e.g. Beam Position Monitors and RF cavities – for about 5% (green to black crosses), and the vacuum flanges and chamber discontinuities for 25% (black to cyan crosses). In total, the imaginary part of the vertical impedance of the SPS is known up to 90% and this is proven also by complementary measurements shown in the following.

The SPS is also an ideal example to illustrate the importance of including the contribution of the quadrupolar impedance in the interpretation of the measurements of coherent tune shift with intensity for a certain machine. Figure 2 shows the expected tune shift with intensity in both the horizontal and vertical planes when the quadrupolar impedance of the SPS (as known from the global impedance model of the machine) is included in the calculation or not.

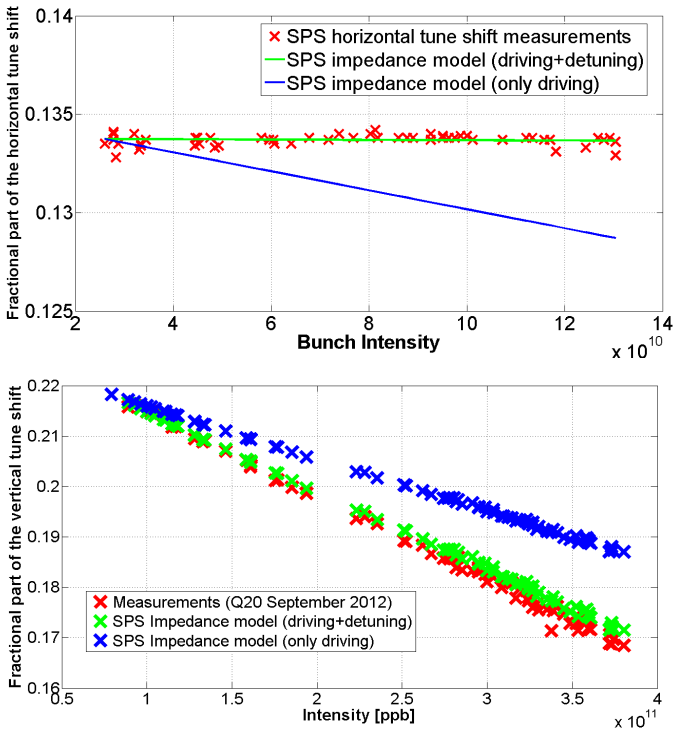

Figure 2: Fractional part of the horizontal (top) and vertical (down) tune as a function of the bunch intensity in the CERN SPS. The blue lines show the expected tune shift with intensity if only the dipolar component of the impedance is included in the calculation.

It is clear that, without the quadrupolar impedance, we would expect roughly similar tune shifts with intensity in both planes (i.e. $\Delta Q_{x,y}/10^{11} \approx 0.05$). However, this value acquires an additional 30% in the vertical plane, while it is basically compensated in the horizontal plane, only due to the contribution of the quadrupolar impedance. The negative quadrupolar impedance in the horizontal plane comes from both the flat vacuum chambers, which occupy more than 60% of the full SPS circumference, and the magnetic kickers (for which the negative quadrupolar impedance is even larger in absolute value than the dipolar one).

Another set of measurements conducted at the CERN SPS is that of the growth rates of the l=0 mode instability for negative chromaticity. Here single bunches with very low intensity (2 x 10^{10} p) were injected into the SPS with a kinetic energy of 25 GeV (γ=27.7), which is above the transition energy of the ring in both optics configurations for which these measurements were carried out (Q20 with γ_t =18 and Q26 with γ_t =23). By setting the

vertical chromaticity to different negative values prior to injection, the beam would become immediately unstable after injection and its rise time could be inferred from the turn-by-turn signal of a position pick up. To interpret these measurements, two different methods were considered: the first one based on the simple application of Eq. (1) with the real part of the impedance as from the global SPS impedance model and the second one based on the reproduction of the observed bunch dynamics by means of the HEADTAIL macroparticle code [4] fed with the wake function associated to the SPS impedance model. The advantage of the second method with respect to the first one was that it would include the possible effects of the nonlinear chromaticity model of the machine as well as the nonlinear longitudinal dynamics of the long bunch in its RF bucket. Figure 3 shows the measured and predicted growth rates in the Q20 (left) and Q26 (right) optics as a function of the chromatic frequency. Due to closer proximity to transition at injection in the Q26 optics, and therefore the lower value of the slippage factor η, obviously the explored frequency range is in this case could be over 3 times larger than in Q20 case.

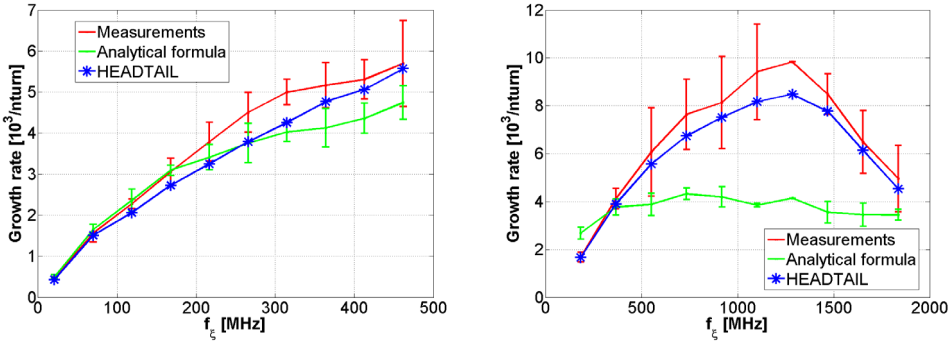

Figure 3: Growth rate of the unstable l=0 mode as a function of the chromatic frequency in the CERN SPS as measured (red), predicted analytically (green) and predicted with macroparticle simulations (blue) in both Q20 (left) and Q26 optics (right).

The agreement between the measurements and the HEADTAIL simulations was found to be excellent for both sets of measurements. The analytical estimation seemed to reproduce closely enough the measured growth rates in the low frequency part, while a discrepancy by up to a factor two was found for higher chromatic frequency shifts. This could be ascribed either to the important influence of nonlinearities in this frequency range, or to the fact that the knowledge of the beam coupling impedance at higher frequencies is not accurate enough to be used in the analytical formula. This is because the impedance model of the SPS was mainly built by means of time domain electromagnetic simulations of the accelerator components and the impedance was then calculated in post-processing by Fourier transforming the wake functions.

2.18.2.2 *Transverse Impedance Measurements with Beam: Transverse Mode Coupling Instability (TMCI) Thresholds*

For higher bunch intensities, the validity of Eq. (1) breaks down. In this regime, radial modes should be also considered in addition to the azimuthal modes, and the shift of the different modes becomes highly nonlinear with the bunch intensity. Above a certain intensity, adjacent modes merge together, or couple, leading to violent headtail instabilities, known as Transverse Mode Coupling Instabilities (TMCI). The threshold intensity at which

this instability sets in has a direct relation with the global transverse impedance of the machine (dipolar plus quadrupolar). Short bunches (i.e. with a l=0 spectrum extending well beyond the impedance spectrum of the accelerator) usually become unstable when modes 0 and -1 couple. This could be intuitively explained mainly for two reasons. First, Eq. (1) shows that the modes shift about like $2^{-|l|}$ (the Gamma function at the numerator and the factorial at the denominator roughly cancel), therefore the modes shifting faster are 0 and ±1. Secondly, we know that the mode 0 shifts downwards, therefore it will couple with -1, which can shift upwards or downwards according to the shape of the imaginary part of the impedance. For long bunches, the situation is more complicated and usually it is higher order modes that lead to a strong coupling and instability. Reference [5] provides analytical formulae that can be applied to predict the onset of TMCI for a bunch under the effect of a broad-band resonator impedance (defined by the parameters: shunt impedance R_T in Ω/m, resonance frequency ω_r, and quality factor Q), in the limiting cases of short and long bunch (with respect to the inverse of the resonance frequency of the resonator):

$$\begin{cases} N < \dfrac{2\pi \cdot 3.75 c Q Q_s \gamma}{\omega_r^2 \sigma_z \bar{\beta}_{x,y} R_T r_{p,e}} & \text{if} \quad \omega_r \sigma_z / c \leq 1 \\ N < \dfrac{2\pi \cdot 5.3 Q^2 Q_s \gamma \omega_r \sigma_z^2}{\bar{\beta}_{x,y} R_T r_{p,e} c^2} & \text{if} \quad \omega_r \sigma_z / c \gg 1 \end{cases} \tag{6}$$

In the above equations, $r_{p,e}$ represent the classical radius of the proton or of the electron, according to whether we are considering a proton or a lepton machine. Written in a differen form, the equations above confirm in essence the empirical criterion that the frequency shift of the lowest headtail mode should remain lower than the synchrotron frequency, but it also adds that this criterion becomes unnecessarily pessimistic for long bunches. The frequency shift only needs to be larger than the synchrotron frequency multiplied by a certain 'mode coupling coefficient', which lies between one and two for short bunches but increases linearly with bunch length for longer ones. If one measures the TMCI threshold in a running machine, a quick estimation of the parameters of the broad-band resonator modeling the global machine impedance can be inferred from the above formulae. Different sets of measurements with different bunch lengths or longitudinal emittances can be used to make the estimation more robust.

Alternatively to this approach, the mode shifting and coupling can be simulated with a full analytical Vlasov solver, e.g. MOSES [6] or DELPHI [7], or extracted from the results of macroparticle codes like HEADTAIL [4], and both the tune shift and the TMCI threshold can be then fitted at the same time. If the impedance model of the machine is complete, then the simulations will closely reproduce the observed behaviour. However, in most practical cases, a discrepancy will be found between the two and an additional broad-band resonator will have to be added to the impedance model to fit the measured data, providing an indication of the missing impedance.

An example of application of this technique to investigate the impedance of a relatively new machine is the measurement of the vertical TMCI threshold at the ALBA synchrotron (Barcelona, Spain) [8]. Figure 4 shows the measured vertical coherent tune shift with single bunch intensity (red points in both plots), up to the point in which the TMCI sets in and beam losses occur, at an intensity value of 9.8 mA. The blue points represent the shift predicted with HEADTAIL simulations by assuming the ALBA impedance model as known (left plot) and after adding to it a broad-band resonator with R_T =1.6 MΩ/m and ω_r = 1 GHz.

The much better agreement of both the coherent tune slope and the TMCI threshold found with the additional broad-band resonator indicates that this resonator is a very reasonable estimation of the missing impedance in the model of the ALBA ring.

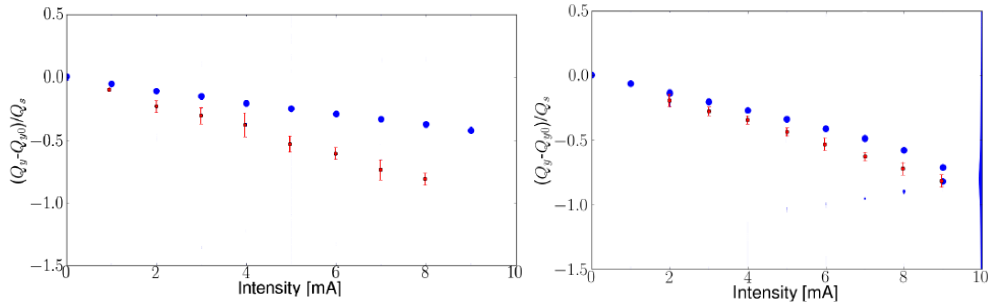

Figure 4: Mode shift as a function of bunch intensity in ALBA as measured (red points) and predicted with macroparticle simulations (blue points) up to the measured TMCI threshold (9.8 mA) with both the bare impedance model of the machine (left) and by adding to it an additional broad-band resonator (right).

TMCI thresholds in a wide range of longitudinal emittances and for the two different optics configurations Q20 and Q26 were also measured for the CERN-SPS and reproduced with HEADTAIL simulations [9]. Figure 5 shows the measured boundary between stable and unstable region for a single bunch in Q26 optics in the plane of longitudinal emittance versus bunch intensity (left) and that simulated with the HEADTAIL macroparticle code using the beam parameters as in the measurement and the SPS impedance model (right). The level of accuracy to which the measurements are reproduced by simulations is yet another confirmation of the advanced knowledge of the transverse impedance of the machine, as was discussed in the previous subsection.

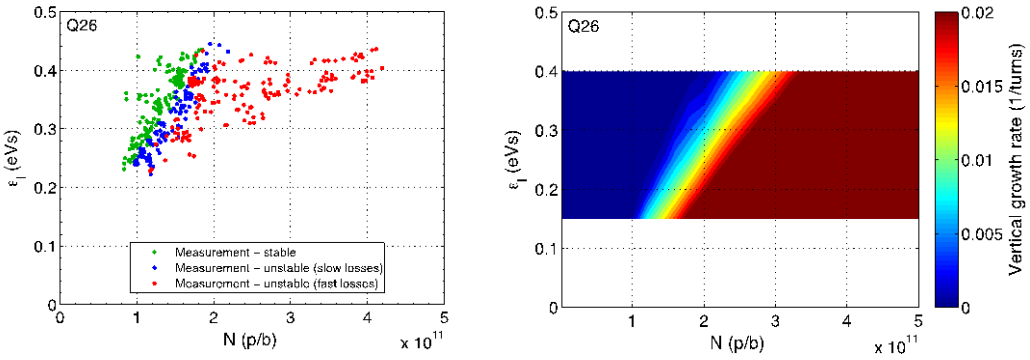

Figure 5: Growth rate of the vertical instability for different bunch intensity/longitudinal emittance pairs as measured in the SPS (left plot, color code in label) and as simulated with the HEADTAIL code (right plot, color code in palette) in Q26 optics

In the case of the Q20 optics, the detailed agreement between measurements and simulations is even more striking. In Fig. 6 the same type of plots as in Fig. 5 are displayed, but for the Q20 optics. In particular, in this case, the simulations are able to reproduce not only the onset of the strong TMCI at very high bunch intensity (red points in the left plot and light blue to red stripe in the right plot, e.g. > 4 x 10^{11} p/b for 0.35 eVs, which is the nominal value of longitudinal emittance for LHC-type beams), but also the island of weak

coupling specially pronounced for low longitudinal emittance values (blue points in the left plot, and region in lighter shades of blue in the plot of the simulations).

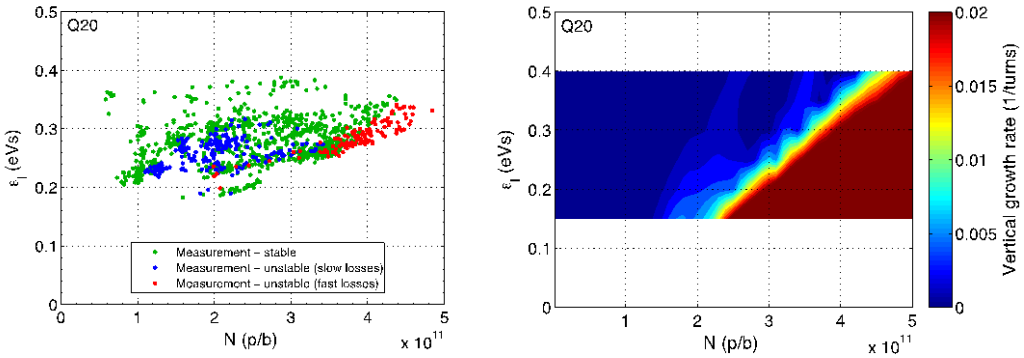

Figure 6: Growth rate of the vertical instability for different bunch intensity/longitudinal emittance pairs as measured in the SPS (left plot, color code in label) and as simulated with the HEADTAIL code (right plot, color code in palette) in Q20 optics.

Another impressive observation about the TMCI with Q20 is that the intra-bunch motion measured with a wide-band pick up is reproduced exactly in simulations for both types of instabilities, which are expected to come from the coupling of different modes. Figure 7 shows measured and simulated intra-bunch traces for the weak instability (top row, showing a quasi mode -1 mode) and for the strong TMCI (bottom row).

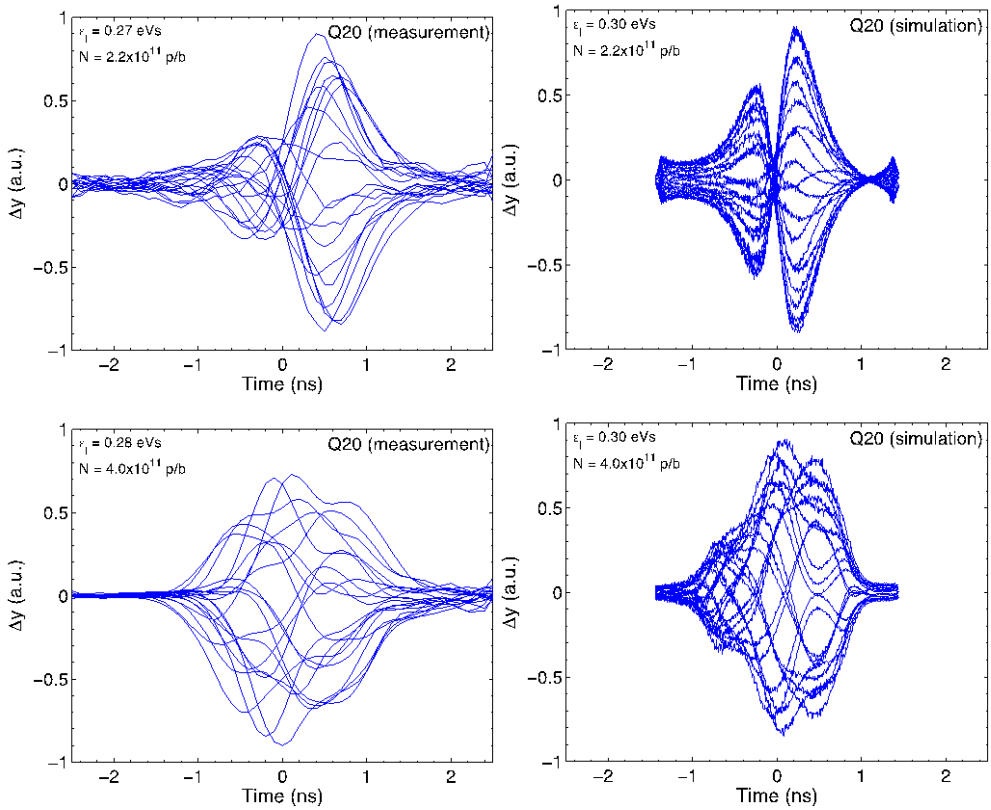

Figure 7: Intra-bunch vertical position signal measured by a wide band pick up on subsequent turns during the instability rise (left plots) for the weak (top) and strong instability (bottom). The corresponding simulated signals are plotted on the right side.

2.18.3 **Longitudinal Impedance Measurements with Beam**

In equilibrium, the distribution of a particle bunch in the longitudinal plane is a function of the Hamiltonian *H* alone, assuming a potential well defined by the total voltage seen by each particle, i.e. the sum of the external and the induced voltage. Including the effect of the induced voltage, which is the convolution of the bunch line density by the longitudinal wake function, or the product of their spectra in frequency domain, leads to what is known as the effect of 'potential well distortion'. By adding the induced voltage to the RF voltage in the linearized longitudinal equation of motion, one can find analytical expressions for both the single particle (incoherent) synchronous phase shift and the synchrotron frequency shift due to the impedance [10, 11]:

$$\begin{aligned} \Delta\phi_s &\approx \frac{Ne\omega_0}{V_{\mathrm{rf}}\cos\phi_s}\sum_n \Lambda_n \mathrm{Re}\left[Z(n\omega_0)\right] \\ \Delta\omega_s &\approx \frac{Ne\omega_0\omega_{s0}}{2V_{\mathrm{rf}}h\cos\phi_s}\sum_n n\Lambda_n \mathrm{Im}\left[Z(n\omega_0)\right] \end{aligned} \tag{7}$$

In the equations above, V_{rf} is the applied RF voltage, ω_{s0} is the unperturbed synchrotron frequency, ϕ_s is the synchronous phase, h is the harmonic number of the RF system, Λ_n are the harmonics of the expansion in Fourier series of the line density $\lambda(z)$, $Z(\omega)$ represents the longitudinal impedance of the machine.

For a reactive impedance $\mathrm{Im}[Z(n\omega_0)]/n$ which is constant over the stable bunch spectrum, the single particle synchrotron frequency shift can be rewritten as a function of the second derivative of the bunch line density at the bunch center in the form

$$\Delta\omega_s \approx \frac{eN\omega_0 C^2 \mathrm{Im}[Z(n\omega_0)]/n}{2V_{\mathrm{rf}}h\cos\phi_s}\left.\frac{d^2\lambda}{dz^2}\right|_{z=0} \tag{8}$$

In this section we will discuss only the beam-based methods for the measurement of longitudinal impedances, which make use of observables related to synchronous phase shift and synchrotron frequency shift. Other methods exist, e.g. based on the measurement of bunch lengthening with intensity, instability thresholds, loss of Landau damping or spectrum of a debunching bunch, but they will not be addressed in this newsletter.

2.18.3.1 ***Incoherent Synchrotron Frequency Shift***

The incoherent synchrotron frequency shift can be found for a bunch in equilibrium by measuring the distance $2m\Delta f_s$ between positive and negative mth synchrotron sidebands of the longitudinal Schottky spectrum [12]. This method was used in both RHIC rings [13], where the dependence on intensity was obtained from the natural intensity decay during luminosity production. The parabolas were fitted to the top 30% of the averaged bunch profiles to find the second derivative of the line density. The results obtained by this method for the two RHIC rings, blue and yellow, which are very similar, differed by more than a factor three and the source of this difference is not clear. The quadrupole (m=2) line of the peak detected Schottky spectrum contains information about the particle distribution in synchrotron frequency [14] and can be used to observe the synchrotron frequency shift. The measurements of m = 2 line performed at bottom energy of the CERN LHC for two bunches

of similar bunch length and different intensity are shown in Fig. 8. As one can see the available frequency resolution of 0.2 Hz is not sufficient and only an upper limit on $\mathrm{Im}[Z(n\omega_0)]/n$ could be obtained ($< 0.2\ \Omega$) [15]. This limit agrees with the current LHC impedance budget of 0.1 Ω.

Another method, which can be used for estimation of the synchrotron frequency shift, when applied in the LHC, gave similar results. Eight bunches with intensities in the range $(0.6 - 2.0) \times 10^{11}$ and bunch length in the range (1.2 –1.4) ns were excited via cavity set point by phase modulation $\phi(t) = \phi_0 \sin(2\pi f_{mod} t)$ with modulation frequency f_{mod} changing in steps of 0.1 Hz from the value above zero-intensity synchrotron frequency f_{s0} = 55.1 Hz. Dipole oscillations of different bunches were observed at excitation frequencies reaching the synchrotron frequency spread inside these bunches. The results are again in agreement with an expected maximum frequency shift of 0.11 Hz. Due to the finite length of this excitation (and therefore frequency bandwidth) a constant offset in synchrotron frequencies was also observed. To improve accuracy longer excitations were applied for shorter bunches (available at the LHC flat top). Finally, the LHC impedance ($\mathrm{Im}[Z(n\omega_0)]/n = 0.09\ \Omega$) could be estimated most accurately from the measurements of thresholds of the loss of Landau damping (for bunches with various lengths and intensities) due to the incoherent synchrotron frequency shift [15], but these results are not discussed in this paper.

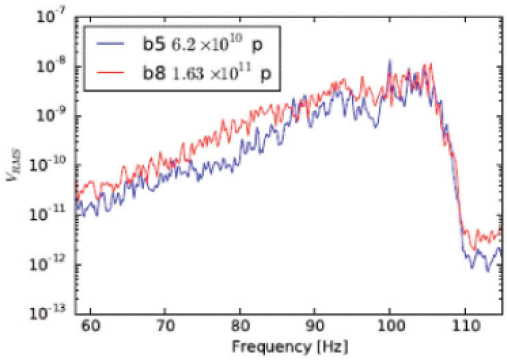

Figure 8: Quadrupole line of the peak detected Schottky signal, proportional to the particle distribution in synchrotron frequency, for two LHC bunches of Beam 1 with similar length of 1.4 ns (**4**σ Gaussian fit) but different intensities between 0.1 and 1:1 x 10^{11} at 450 GeV/c (f_{s0} = 55.1 Hz). The difference 2δfs is below 1.0 Hz and δfs = 0.35 Hz is expected from the LHC impedance model.

2.18.3.2 *Coherent Synchrotron Frequency Shift*

The synchrotron frequency shift can also be measured from excited oscillations of bunches with different intensities N. In this case we are dealing with the coherent synchrotron frequency shift as well as with the incoherent spectrum since now the bunch spectrum consists of both stationary and oscillating components. The frequency of bunch oscillations can be presented in the form

$$\omega_m = m(\omega_{s0} + \Delta\omega_{inc}) + \Delta\omega_{col} \tag{9}$$

where $\Delta\omega_{inc}$ and $\Delta\omega_{coh}$ are correspondingly the incoherent and coherent synchrotron frequency shifts. The two last terms in the equation above are defined by the two different effective impedances. In fact, while the incoherent frequency shift $\Delta\omega_{inc}$ is proportional to $\mathrm{Im}(Z_0)$, the coherent frequency shift $\Delta\omega_{coh}$ is proportional to $[\mathrm{Im}(Z)/\omega]_m^{eff}$, where

$$[\mathrm{Im}(Z)/\omega]_m^{\mathrm{eff}} = \frac{\sum_{p=-\infty}^{\infty} h_m(\omega_{pm}) Z(\omega_{pm})/\omega_{pm}}{\sum_{p=-\infty}^{\infty} h_m(\omega_{pm})} \tag{10}$$

with $\omega_{pm}=p\omega_0+m\omega_s$. The spectral functions $h_m(\omega)$ were defined in the previous subsection. For dipole oscillations (m = 1) the last two terms in the equation for the longitudinal modes of the single bunch oscillation frequency practically cancel each other (exactly for a parabolic bunch in a linear RF voltage). So for beam measurements we are left with quadrupole (m = 2) oscillations, which, for example, can be excited at injection into a mismatched RF voltage or by nonadiabatic increase of voltage. The frequency of bunch length (or bunch peak amplitude) oscillations can be found from fitting the measured oscillations with a sine-wave. The variation of bunch intensity allows the dependence of oscillation frequency on impedance to be estimated using the expression

$$\omega_{2s} = \omega_{2s0} + bN \tag{11}$$

where for Im*(Z)/n=const* the slope *b* is proportional to Im*(Z)/n*. Note that the slope *b* also strongly depends on bunch length (like $1/\sigma_z^3$ for Im*(Z)/n=const*) and special care should be taken when performing the reference impedance measurements, as in the CERN SPS [16], by using bunches with similar bunch lengths and longitudinal emittances. Indeed single bunches injected into mismatched voltage at 26 GeV/c (above transition) have been used in the CERN SPS to evaluate changes in longitudinal inductive impedance since 1999, see Fig. 9 (left). The first significant reduction in the inductive impedance (the slope *b*) could be seen after shielding the ~900 pumping ports in 2000 (compare measurements from 1999 and 2001) followed by impedance increase due to installation in 2003 and 2006 of kickers for beam extraction to the two LHC rings. Later the impedance of a few kickers was significantly reduced, but the effect was not measurable with beam anymore [16], mainly due to bunch length variation in measurements. Recently measurements of synchrotron frequency shift as a function of bunch length allow the frequency dependence of effective impedances to be studied as well, see Fig. 9 (right). Comparison of these measurements with particle simulations can serve as a good test of the impedance model of the ring. In the case of the CERN SPS this comparison reveals some missing inductive impedance Im*(Z)/n*~0.3 Ω [17]. The analysis also shows that for the SPS impedance measured using the quadrupole oscillations, the frequency shift is dominated by the contribution from the incoherent frequency shift.

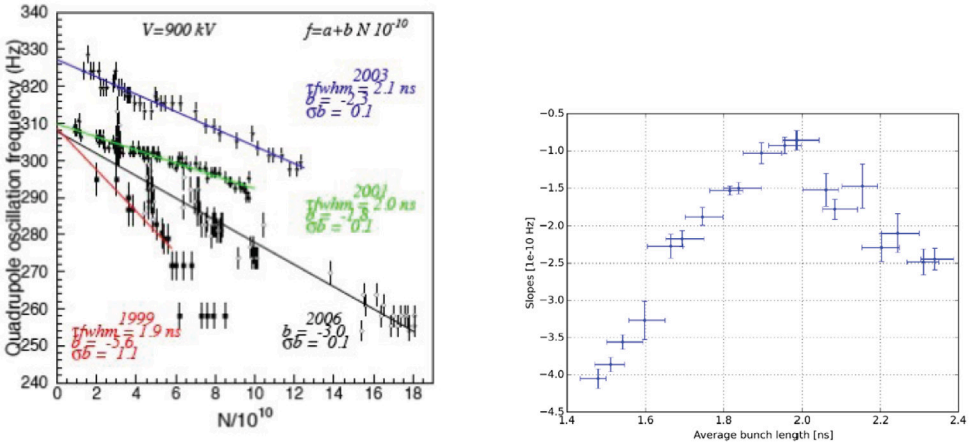

Figure 9: Left: measurements of quadrupole frequency shift as a function of intensity (slope b) over few years in the CERN SPS following the impedance evolution of the ring. Right: recent measurements of the slope b in [Hz/10^{10}] as a function of average bunch length.

2.18.3.3 *Synchronous Phase Shift*

Measurements of the synchronous phase shift as a function of intensity are often used for the evaluation of the resistive impedance of a ring [18]. The shift of the synchronous phase ϕ_s is defined by the expression

$$\Delta\phi_s = -\frac{U}{eV_{\mathrm{rf}}\cos\phi_s} \tag{12}$$

where U is energy loss per turn and per particle. The first equation in Section 2.17.3 describes the phase shift of a single particle with a small synchrotron oscillation amplitude. In the same way as the energy loss of a given particle, this phase shift depends on the particle oscillation amplitude. Experimentally only the total energy loss of the whole bunch can be measured. The total energy loss normalised to the number of particles can be found by measuring the synchronous phase shift $\Delta\phi_s$ at different bunch intensities. The measured dependence of energy loss on bunch length can be compared with that calculated from the known resistive impedances and the given bunch distribution. The energy loss of the whole bunch per turn and per particle can be found from the following expression

$$\Delta\phi_s = \frac{Ne\omega_0}{\pi V_{\mathrm{rf}}\cos\phi_s}\sum_{p=0}^{\infty}\mathrm{Re}[Z(p\omega_0)]|\Lambda(p\omega_0)|^2 \tag{13}$$

The shift of the synchronous phase $\Delta\phi_s$ can be measured from the distance between the two bunches in the ring or from the phase of beam signal relative either to the reference RF signal or to the signal from a probe in the RF cavity. When using the reference RF signal (sent from the power amplifier to the cavity) the energy loss due to the cavity fundamental impedance is included. The signal from the probe in the cavity contains information about the sum of applied RF voltage and beam induced voltage, so that in this case the beam-loading effect will be excluded from the measured phase shift. Measuring the distance between a time reference, low intensity bunch, and a witness bunch with varied intensity

(see e.g., [19]) is similar to the use of the reference RF signal since the measured loss factor can be dominated by the contribution from the RF cavities.

The measurements of synchronous phase shift done in the CERN SPS after the first impedance reduction using the RF reference signal [20] are shown in Fig. 10. Single bunches with variable intensity were injected in 4 different RF voltages to obtain the dependence of energy loss on bunch length. In the measurements $\sigma_t=\sigma_z/(\beta c)$, with β being the relativistic factor, varied in the range (0.6-0.9) ns so that impedances up to 1 GHz should be taken into account. Contributions to the normalised energy loss $|U|/(N/10^{10})$ from different SPS impedances below 1 GHz (at the time of measurements) calculated for a Gaussian bunch are shown in Fig. 10 (left). As can be seen, in these measurements the energy loss was dominated by the loss in the fundamental impedance of the 200 MHz RF system (shunt impedance R_{sh}~4.5 MΩ, quality factor Q = 140) and the MKE kickers. Contributions due to the main impedance of the 800 MHz cavities, total R_{sh} = 1.94 MΩ and Q = 300, as well as the HOM of the 200 MHz RF system, with f_r = 629 MHz, Q = 500 and R_{sh} = 604 kΩ are much smaller. The contribution to the energy loss from the resistive wall impedance is about 0.8 keV for a bunch with σ_t = 0.6 ns and decreases like $\sigma_t^{-3/2}$ for longer bunches. The measured and estimated total energy losses are presented in Fig. 10 (right) as a function of bunch length.

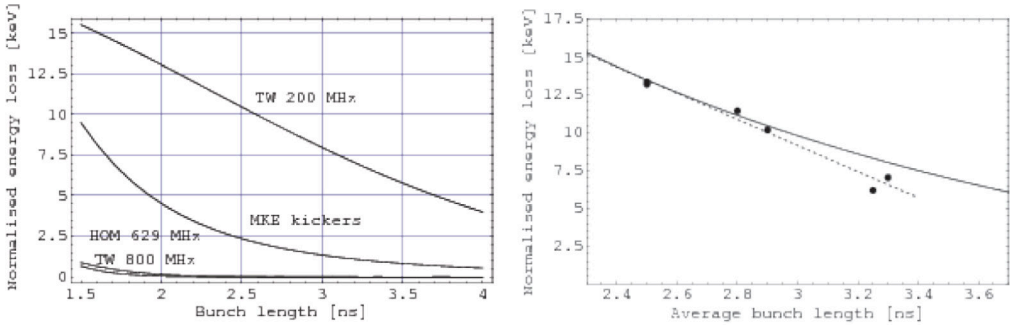

Figure 10: Left: contribution to energy loss (keV) from different SPS impedances as a function of $4\sigma_z$ bunch length. Right: Normalised energy loss (keV) calculated from the known SPS impedances (solid line) and measured from the phase shift (circles – measurement points, dashed line – their linear fit) for different bunch lengths.

The bunch-by-bunch measurements of the beam phase relative to the measured RF phase (probe) were used in the CERN LHC to estimate the energy loss of the proton bunches due to the electron cloud. Very high accuracy, below one degree, is required to accurately measure the small shifts. To obtain reliable results the first 12 bunches were used as a reference to exclude other energy losses, from (short range) impedances. The required accuracy was achieved after corrections for systematic errors and data post-processing [15]. Comparison with simulations gives a good estimate of the e-cloud density, as is discussed in deeper detail in the section of this newsletter devoted to electron cloud. From 2015 this diagnostic tool is available in the CERN Control Center and used for evaluation of results of beam scrubbing of the vacuum chamber (see Fig. 12).

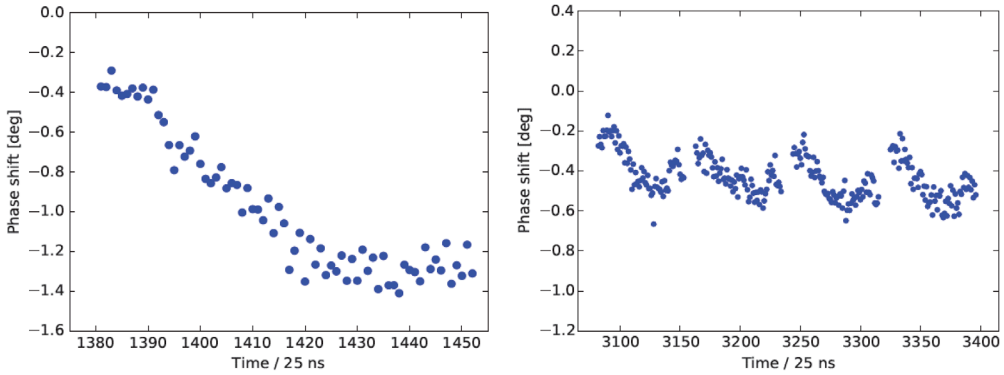

Figure 11: Bunch-by-bunch synchronous phase shift for similar bunches spaced at 25 ns before (left) and after (right) scrubbing of the CERN LHC. Measurements at 450 GeV/c flat bottom.

2.18.4 Acknowledgements

The authors would like to thank T. Argyropoulos, H. Bartosik, T. Bohl, H. Damerau, J. Esteban-Müller, E. Koukovini-Platia, G. Iadarola, A. Lasheen, K. Li, T. Linnecar, N. Mounet, H. Timkó and C. Zannini for their invaluable contributions.

2.18.5 References

1. A. W. Chao, "Physics of Collective Beam Instabilities in High Energy Accelerators", Editor John Wiley & Sons, Inc. 1993
2. G. Rumolo, "Beam Instabilities" in Proc. of CAS, Advanced Accelerator Physics Course, 18 – 29 August 2013, Trondheim, Norway, p. 199
3. C. Zannini, "Electromagnetic Simulation of CERN accelerator Components and Experimental Applications", CERN-THESIS-2013-076 (2013)
4. G. Rumolo and F. Zimmermann, "Practical User Guide for HEADTAIL", CERN-SL-Note-2002-036-AP (2002)
5. B. Zotter, "Transverse Mode Coupling and Headtail Turbulence", CERN/ISR-TH/82-10 (1982)
6. Y. H. Chin, "Transverse Mode Coupling Instabilities in the SPS", CERN-SPS-85-2-DI-MST (1985)
7. N. Mounet, "DELPHI: an analytical solver for impedance driven modes", CERN-ACC-SLIDES-2014-0066 (2014)
8. E. Koukovini-Platia, "High Frequency Effects of Impedances and Coatings in the CLIC Damping Rings", CERN-THESIS-2015-152 (2015)
9. H. Bartosik, "Beam dynamics and optics studies for the LHC injectors upgrade", CERN-THESIS-2013-257 (2013)
10. J. L. Laclare, "Bunched beam coherent instabilities", Proc. of CERN Accelerator School (CAS) 1985, CERN 87-03, p. 264 (1987)
11. J. Haissinski, Nuovo Cimento 18 B 72 (1973)
12. D. Boussard, "Schottky noise and beam transfer function diagnostics", Proc. of CERN Accelerator School (CAS) 1985, CERN 87-03, p. 416 (1987)

13. M. Blaskiewicz, J. M. Brennan and K. Mernick, “Longitudinal impedance of RHIC”, Proc. IPAC2015, Richmond, VA, USA, p. 746 (2015)

14. E. Shaposhnikova, T. Bohl and T. Linnecar, “Longitudinal peak detected Schottky spectrum”, Proc. HB2010, Morschach, Switzerland, p. 363, TUO1C04 (2010)

15. J. Esteban Muller, Ph.D. Thesis, EPFL, Lausanne, Switzerland (2016)

16. E. Shaposhnikova *et al*., “Reference measurements of the longitudinal impedance in the CERN SPS”, Proc. PAC09, Vancouver, Canada, (2009)

17. A. Lasheen *et al*., “Single bunch longitudinal instability in the CERN SPS”, Proc. IPAC2016, p.1670, TUPOR009, Busan, Korea (2016)

18. M. A. Allen, J. M. Paterson, J. R. Rees, P. B. Wilson, IEEE, NS-22, No.3, p. 1838 (1975)

19. N. S. Sereno *et al*., “A potpourri of impedance measurements at the Advanced Photon Source Storage Ring”, Proc. PAC97, p. 1700 (1997)

20. E. Shaposhnikova, T. Bohl, A. Hofmann, T. Linnecar, J. Tuckmantel, “Energy loss of a single bunch in the CERN SPS”, Proc. EPAC04, Lucerne, Switzerland and CERN AB-Note-2004-017-RF (2004)